

# Quantum effects in accumulation and inversion layers of narrow-gap and gapless $\text{Hg}_{1-x}\text{Cd}_x\text{Te}$

V. F. Radantsev, T. I. Deryabina, L. P. Zverev, G. I. Kulaev, and S. S. Khomutova

*A. M. Gor'kii Ural State University*

(Submitted 2 November 1984)

Zh. Eksp. Teor. Fiz. **88**, 2088–2107 (June 1985)

The two-dimensional gas of surface electrons in  $\text{Hg}_{1-x}\text{Cd}_x\text{Te}$  ( $0.09 \leq x \leq 0.22$ ) is investigated by capacitive spectroscopy in quantizing magnetic fields. The cyclotron masses and subband populations are measured and the coupling energies and dispersion laws are determined for the subbands. The effects caused by the degeneracy of the bulk electrons in accumulation layers are investigated. Screening by free electrons is found to cause oscillations in magnetic fields parallel to the surface. Experiments in inclined fields indicate that (as in Si) the spin splitting is determined by the total magnetic field, and the  $g$ -factors are found. Localization of electrons by the magnetic field is observed for the most heavily doped materials. The minima in  $C(H)$  for the  $N = 1, 2$  Landau levels in weakly doped materials occur at fields for which the filling factors are multiples of  $1/3$ .

## 1. INTRODUCTION

The quantum phenomena in the inversion and accumulation layers of narrow-gap semiconductors differ in several respects from their more familiar counterparts for silicon surface layers. Because of the small effective mass in narrow-gap semiconductors, several dimensionally quantized subbands are generally filled even for surface electron densities as low as  $n_s \sim 10^{12} \text{ cm}^{-2}$ . Since the conduction band is appreciably nonparabolic, the components of the electron motion normal and parallel to the surface are mixed, so that the density of states depends on the absolute energy of the bottom of the  $2D$ -subbands as well as on the energy relative to the bottom of the subband. Some theoretical aspects of this problem were recently considered in Refs. 1–3.

Most current experimental work is concerned with the “classical” narrow-gap semiconductors InSb and InAs. Quantum effects in the surface layers of semiconductors with narrower band gaps  $E_g$  have been studied much less systematically,<sup>4,5</sup> and virtually no work has been done on gapless semiconductors. Nevertheless, these materials are of particular interest, partly because they exhibit the quantum effects most strongly, and partly because their behavior is unusual in other ways. Specifically, for gaps  $E_g < 80 \text{ meV}$  the wave functions of the surface electrons do not decay within the depletion layer, because of the small width of the latter; the wave functions thus have “tails” that extend out to the valence band in the bulk of the semiconductor.<sup>1</sup> The electron states are then resonant in the surface layer, and all the more in negative-gap materials. The electrons can thus tunnel across the barrier between the inversion channel and the bulk material. The resultant shunting of the channel by the bulk material makes it difficult to study the accumulation and inversion layers by conventional galvanometric techniques, and this is one of the reasons why few experiments have been carried out for these materials.

We avoid these difficulties in our present work by employing an alternative method based on measuring the differential capacitance of the space-charge region (SCR) in

quantizing magnetic fields. When exposed to a quantizing combined electric and magnetic field normal to the surface of a semiconductor, the electron-gas spectrum in the SCR degenerates into two-dimensional subbands in which the density of states oscillates with energy. Let  $Q_s$  be the charge stored in the SCR and  $\varphi_s$  be the surface potential, which determines the position of the Fermi level. Since the density of states in the  $2D$ -subbands at the Fermi level oscillates with  $\varphi_s$ , the differential capacitance  $C_s \equiv dQ_s/d\varphi_s$  of the SCR also oscillates with the magnetic field and with the band bending at the surface, which in turn is determined by the strength of the electric field. The periods and the amplitudes of the oscillations of  $C_s$  are determined by the density of states and by the position of the Fermi level in the  $2D$ -subbands; measurements of the oscillations can therefore yield detailed information about the electron energy spectrum in the SCR. Unlike methods based on measuring the conductivity, which cannot be employed when the surface channels are shunted by the bulk material, the capacitive method can be used to study both inversion and accumulation layers in arbitrarily doped semiconductors (including semiconductors with a negative gap).

In this paper we use the capacitive technique to study inversion and accumulation layers in narrow-gap and gapless  $\text{Hg}_{1-x}\text{Cd}_x\text{Te}$  ( $0.09 \leq x \leq 0.22$ ). We selected this material because its band parameters (in particular, the energy gap  $E_g = E(\Gamma_6) - E(\Gamma_8)$  between the  $\Gamma_6$ - and  $\Gamma_8$ -bands) can be changed by varying the composition  $x$ ; in addition, the energy spectrum of the bulk electrons is fairly well known.

## 2. DESCRIPTION OF THE SAMPLES AND EXPERIMENTAL PROCEDURE

Table I lists the composition, band parameters, conductivity type, and doping density of the samples at  $T = 4.2 \text{ K}$ . To eliminate errors in determining  $x$  caused by possible inhomogeneity of the  $\text{Hg}_{1-x}\text{Cd}_x\text{Te}$  alloys, we employed tun-

TABLE I.

Sample No.	$x$	$E_g$ , meV	$\frac{m_n}{m_0} \cdot 10^3$	type	$ N_D - N_A $ cm <sup>-3</sup>	$i$	$n_{si} \cdot 10^{-11}$ , cm <sup>-2</sup>	$dn_i/dn_s$	$\frac{m_c i}{m_0} \cdot 10^3$ ( $n_s = 2 \cdot 10^{12}$ cm <sup>-2</sup> )
1	0,215	85	7,5	<i>n</i>	$3,2 \cdot 10^{14}$	0	0	0,690±0,005	43±2
						1	0	0,231±0,002	25±2
						2	1,4±0,2	0,079±0,003	
2	0,22	100	9,0	<i>n</i>	$3,0 \cdot 10^{16}$	0	1,5±0,05	0,704±0,003	—
						1	3,2±0,15	0,224±0,003	—
						2	10±1	0,076±0,003	—
3	0,22	100	8,9	<i>p</i>	$2 \cdot 10^{14}$	0	0	0,700±0,004	45±3
						1	3,6±0,01	0,227±0,002	25±2
						2	14,7±2,0	0,074±0,003	
4 [3] theory	0,22	104	8,7	<i>p</i>	$1 \cdot 10^{14}$	0	0	0,61	38,7
						1	0,3	0,24	27,3
						2	2,7	0,1	18,9
						3	4,8	0,04	
5 **	0,215	85	7,5	<i>p</i>	$9,1 \cdot 10^{17}$	0	0	0,680±0,004	—
						1	7,3±0,3	0,240±0,004	—
						2	35,6±3	0,079±0,003	—
6	0,125	-50	4,1	<i>n</i>	$3,5 \cdot 10^{15}$	0	0,42±0,07	0,652±0,003	43±2
						1	1,1±0,1	0,230±0,002	26±2
						2	4,4±0,4	0,076±0,002	17±2
						3	11,1±2	0,041±0,005	
7	0,12	-55	4,0	<i>n</i>	$1,8 \cdot 10^{16}$	0	1,1±0,05	0,670±0,005	—
						1	3±0,1	0,228±0,004	—
						2	8,8±0,5	0,077±0,002	—
						3	24±3	0,025±0,005	—
8	0,11	-70	6,1	<i>n</i>	$5,0 \cdot 10^{16}$	0	2,1±0,05	0,700±0,005	44±2
						1	4,3±0,1	0,220±0,004	27±2
						2	13,2±1	0,078±0,002	17±3
9 ***	0,09	-100	9,0	<i>p</i>	$1,4 \cdot 10^{18}$	0	0	0,768±0,005	46±2
						1	12,5±0,5	0,232±0,003	27±2

\*Found from  $C$ - $V$  measurements.

\*\*Obtained by annealing sample 1 isothermally for 24 h at 380 °C.

\*\*\*The Hall constant for this sample changed sign at  $H \approx 1$  kOe; the value cited for  $N_A - N_D$  was found from Hall measurements near saturation.

nel spectroscopy in quantizing magnetic fields<sup>6</sup> to find the gap  $E_g$  and the effective mass  $m_n$  of all the samples at the bottom of the conduction band. The carrier density  $|N_A - N_D|$  was deduced from measurements of the Hall voltage (in addition, tunneling and the Shubnikov measurements were made for  $n$ -type materials with  $n > 10^{15}$  cm<sup>-3</sup>).

The MOS structures were fabricated from Hg<sub>1-x</sub>Cd<sub>x</sub>Te wafers passivated by anodic oxidation. The area of the gate region was typically 10<sup>-3</sup> cm<sup>2</sup>. Because the dielectric constant was large ( $\epsilon \sim 20$ ) and the oxide layer was thin ( $d = 600$ – $1500$  Å), high surface carrier densities up to 10<sup>13</sup> cm<sup>-2</sup> were achieved at relatively low gate voltages  $V = 10$ – $15$  V. The samples were mounted in a holder and placed inside a cryostat (temperature adjustable from 4.2 to 77 K), and the magnetic field  $H \leq 60$  kOe was generated by a superconducting solenoid.

We measured the capacitance  $C$  of the MOS structures by the resonant null method. The amplitude of the test signal was equal to 10 mV, and the frequency  $f$  ranged from 3·10<sup>3</sup> to 5·10<sup>6</sup> Hz. We tested 5–10 MOSFET transistors fabricated from each of the samples. Variations in the properties of the batch of transistors fabricated from the same sample will be neglected, since they have no influence on the physical effects discussed below.

### 3. $C$ - $V$ CHARACTERISTICS AND CAPACITANCE MAGNETOOSCILLATIONS

Because no gap separated the majority and minority carrier bands, the capacitance-voltage ( $C$ - $V$ ) characteristics of the gapless semiconductor structures exhibited a typical low-frequency behavior at all temperatures and frequencies. In addition, the experimentally observed capacitance modulation was substantially less than the calculated value at all frequencies, possibly because of contributions from the capacitance of states at the interface (for gapless semiconductors, the energy of these states overlaps some of the allowed bands, i.e., they are resonant surface states).

For positive-gap samples ( $E_g > 0$ ),  $C(V)$  also had the typical low-frequency form at all temperatures for  $f < 0.05$  MHz; for  $f > 0.3$  MHz and  $T < 15$  K the capacitance plot takes the form of a shelf at small band bending due to inversion. The form of the  $C$ - $V$  characteristics and the behavior of the resistive component of the admittance as functions of frequency and temperature indicate that carriers were exchanged rapidly between the inversion layer and the bulk material even for  $T = 4.2$  K and gap widths  $E_g = 0.1$  eV. This indicates that tunneling from deep levels in the depletion predominates.

In all cases, the  $C$ - $V$  characteristics oscillated as the magnetic field varied, and the field component  $H_{\perp} = H \cos \alpha$  normal to the oxide interface determined the oscillation period (here  $\alpha$  is the angle between  $\mathbf{H}$  and the normal to the interface).

The capacitance  $C(V_G)$  peaked whenever the Fermi level intersected one of the Landau levels (the  $N$ th, say) in one of the subbands (the  $i$ th, say); in terms of the surface density  $n_i$  of carriers in the  $i$ th subband, the peaks occurred when

$$n_i = g_s \frac{eH_{\perp}}{ch} (N+1), \quad (1)$$

where  $eH_{\perp}/ch$  is the degeneracy of the Landau level, and  $g_s$  is the spin degeneracy. The experimental observations indicate that the population rate  $dn_i/dn_s$  of 2D subbands was constant for sufficiently large  $n_s = \sum n_i$ ; in this case we have

$$n_i = \frac{dn_i}{dn_s} (n_s - n_{si}),$$

where  $n_{si}$  is the surface density of the carriers at the start of the  $i$ th subband. Since

$$n_s = N_s = \frac{C_{ox}}{e} (V - V_{FB} - \varphi_s) \quad (2)$$

if localization effects are neglected (here  $C_{ox}$  is the specific capacitance of the oxide,  $V$  is the applied voltage,  $V_{FB}$  is the flat-band voltage for accumulation layers or the threshold

voltage for inversion layers), the voltages  $V$  corresponding to the oscillation peaks are therefore given in terms of the field  $H$  by

$$V = V_{si} + \varphi_s + \frac{1}{C_{ox}} \left( \frac{dn_i}{dn_s} \right)^{-1} \frac{e^2 g_s}{ch} \left( N + \frac{1}{2} \right) H_{\perp}, \quad (3)$$

where  $V_{si} = V_{FB} + en_{si}/C_{ox}$  is the voltage at the start of the  $i$ th subband. Because of the large permittivity of the oxide in our structures, we have retained  $\varphi_s$  in Eqs. (2) and (3), since otherwise an error of 5–7% in  $N_s$  will result (we note however that  $\varphi_s$  can generally be neglected for  $\text{SiO}_2$ -Si structures). We calculated the surface bending of the bands by solving the Poisson equation for a classical SCR in the two-band Kane approximation. Comparison with the self-consistent calculation in Ref. 3 indicates that neglecting the dimensional quantization causes an error of  $\sim 10\%$  in  $\varphi_s$ , which is perfectly acceptable since  $\varphi_s$  itself is just 5–7% of  $V - V_{FB}$ .

Figure 1 shows a fan diagram for the peaks in  $dC/dV$  expressed in  $V$ - $H$  coordinates; the number  $i$  labels the subbands, and the curves are labeled by the corresponding number  $N$  of the Landau levels in the  $i$ th subband. The oscillations in  $dC/dV(H)$  are also shown for two fixed gate voltages  $V$  for sample No. 3. Oscillations corresponding to three-dimensional subbands are observed, along with spin splitting in the  $i = 0$  subband for Landau levels with  $N < 4$ . According

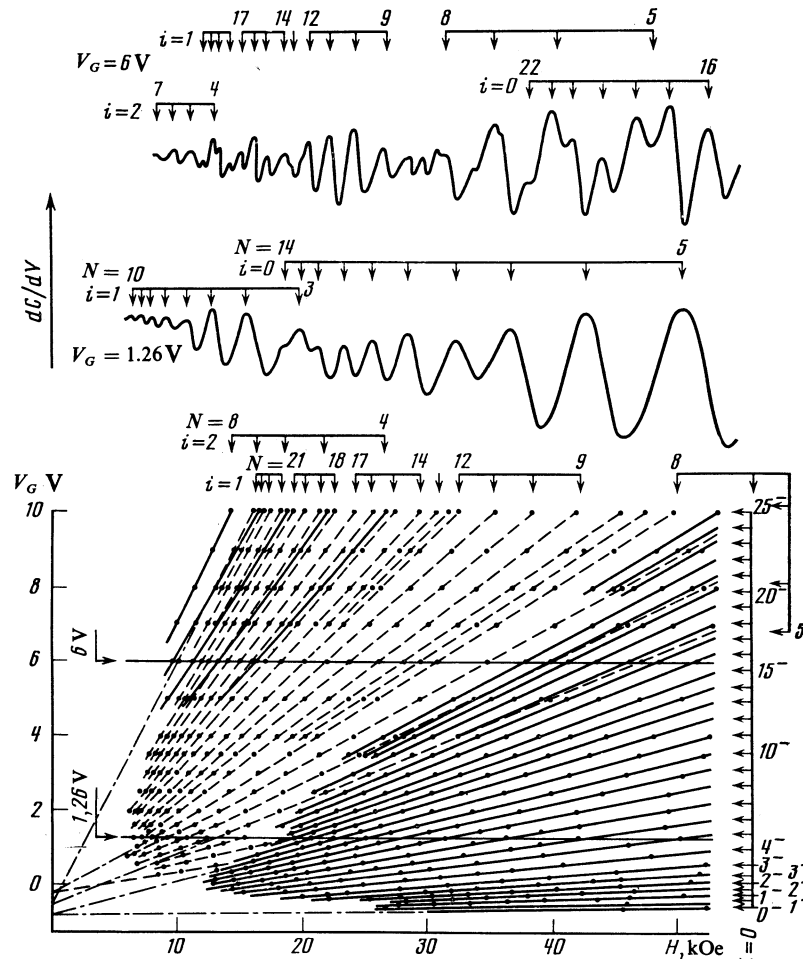


FIG. 1. Magnetooscillations in  $dC/dV$  and peak positions as a function of the gate voltage  $V_G$  for sample 3. The curves are labeled by the corresponding Landau level numbers  $N$ , and the superscripts + and - indicate states with spin  $s = +1/2$  and  $-1/2$ , respectively.

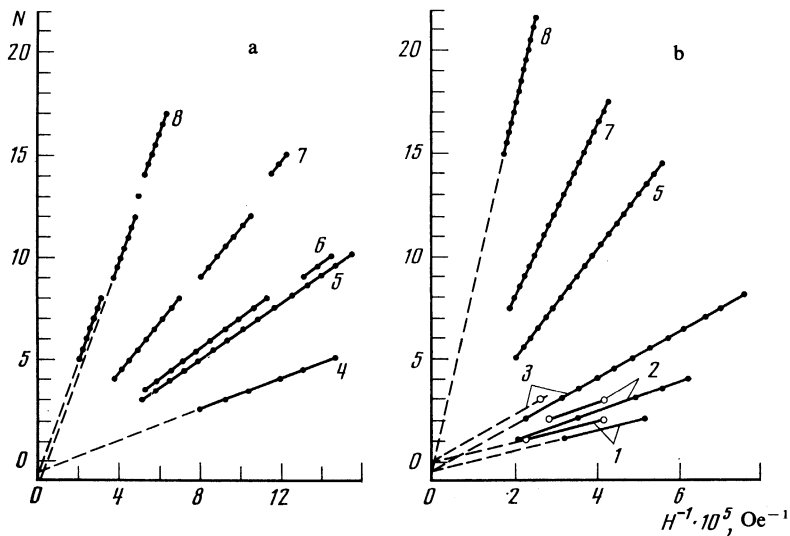


FIG. 2. Fan diagrams for oscillations in the  $i = 1$  (a) and  $i = 0$  2D-subbands (b) for the same structure as in Fig. 1.  $N$  is the Landau level number and  $H^{-1}$  is the reciprocal of the magnetic field;  $C(V_G)$  has minima at half-integral values of  $N$ . The gate voltage  $V_G$  is: 1) 0.48; 2)  $-0.31$ ; 3) 0; 4) 0.8; 5) 1.26; 6) 1.4; 7) 2.5; 8) 6.0 V.

to Fig. 2, the oscillations in the  $i = 1$  subband can be grouped into several series (see also Fig. 1) which have different phases but nearly equal periods with respect to  $1/H$ . For all  $V$ , the phase jumps are nearly equal to  $\pm \pi$  and occur in the same Landau levels (with the same  $N$ ). The oscillation amplitude also behaves anomalously near the phase jumps, and secondary dips and "false" maxima are present. Oscillation phase jumps in the  $i = 1$  subband were observed for all of the samples; phase jumps also occurred in the  $i = 2$  subband for those samples in which the  $i = 3$  subband was populated. The oscillations associated with the  $i = 0$  subband do not undergo any pronounced changes of phase (except for samples 5 and 9); however, the anomalous behavior of the oscillation amplitudes persists even in this case (see, e.g., level  $N = 8$  in Fig. 1).

The phase jumps cannot be ascribed to spatial variations in the surface density of the carriers, because they occurred in all the MOSFETs regardless of the oxide thickness, gate area, or built-in charge density. Moreover, the oscillations near the phase jumps behaved in the same way for all of the MOSFETs fabricated from the same sample.

We attribute the abrupt changes in the oscillation phase to filling of the first few 2D-subbands. According to (1),  $n_i$  must be independent of  $H$  if the oscillations are to be periodic in  $1/H$ . In this case the Fermi energy  $E_F$  oscillates and the Fermi surface "jumps" down to a lower level  $N'$  when the current Landau level  $N > N'$  becomes depopulated as  $H$  increases. If several subbands are filled, jumps in the highest subband can distort the Fermi surface in the lower subband(s) and therefore change the phase of the oscillations there. This mechanism is consistent with the experimentally observed behavior of the oscillations. Indeed, the phase jumps are periodic in  $1/H$ , and the period is nearly identical to the oscillation period in the next higher subband  $i + 1$ . No phase jumps are observed for voltages  $V$  less than the voltage  $V_{si+1}$  corresponding to the start of the next subband; however, the phase jumps are clearly present for large  $V$ .

However, the nature of the phase jumps is not entirely clear. For instance, the behavior of the oscillation curves  $C(H)$  in the inversion layers of the heavily doped samples 5

and 9 is abnormal; unlike the other samples, in this case the jumps occur even before the start of the next subband and involve different Landau levels  $N$  as  $n_s$  varies. Perhaps this is due to carrier exchange between the inversion layer and the depletion region as  $H$  varies.

The phase jumps apparently occur only in materials with small gaps  $E_g$ . Indeed, we also carried out the same measurements on accumulation layers in InAs ( $n = 2 \cdot 10^{16}$  or  $2 \cdot 10^{17} \text{ cm}^{-3}$ ) but did not observe phase jumps or other abnormal behavior of the oscillation amplitude in any of the three two-dimensional subbands.

#### 4. POPULATIONS OF THE SUBBANDS. LOCALIZED STATES

Figure 3 plots the surface carrier density as a function of the gate voltage  $V_G$  for sample 3; the density  $n_i$  in the  $i$ th subband was deduced from the oscillation period  $\Delta_i$  by the formula  $n_i = e/c\pi\hbar\Delta_i$ . We note with regard to this formula that the periods  $\Delta_i$  differed somewhat for portions of the oscillating curves  $C(H)$  with different phases. Specifically,  $\Delta_i$  found for Landau levels  $N \leq 7$  was 2–5% less than for  $7 < N < 11$ . The phase jump involving Landau levels 7–8 is thus apparently accompanied by a change in  $n_i$ . Unfortunately, the large error in determining  $\Delta_i$  for small  $H$  prevents us from reaching any definite conclusion regarding the behavior of  $\Delta_i$  for phase jumps involving large Landau numbers  $N$ . To within the experimental error, the period  $\Delta_{i=0}$  for the lowest subband was the same both before and after the phase jump (in those samples where a jump occurred). The surface densities  $n_i$  in Fig. 3 for subbands with phase jumps were calculated from the values of  $\Delta_i$  found for small  $N$ . However, since the excited subbands can account for at most one-third of all the occupied states, the difference in  $\Delta_i$  should cause little error in the total surface carrier density.

Figure 3 also shows the total surface density  $n_s = \sum n_i$  of electrons in the 2D-subbands and the total density  $N_s$  of induced carriers. We see that  $N_s > n_s$  for all gate voltages, which implies that some of the induced carriers are in localized states, i.e., in states that are not subject to Landau quantization. The carrier density  $N_s - n_s$  in the localized states

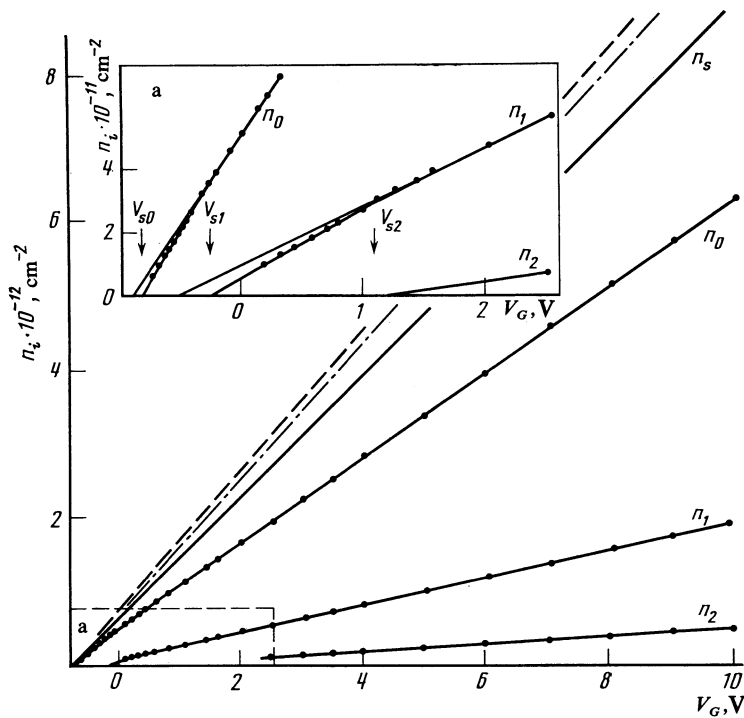


FIG. 3. Concentration  $n_i$  vs gate voltage for sample 3. The dashed line shows  $N'_s = e^{-1}C_{ox}(V_G - V_{FB})$ ; the dashed-and-dotted line plots  $N_s = e^{-1}C_{ox}(V_G - V_{FB} - \varphi_s)$ . The insert *a* shows the lower left-hand corner to larger scale.

increases with  $V_G$ . Moreover, the localized states are resonance states, because the electron gas is degenerate near the surface and only states below the bottom of the conduction band can be filled. The resonance states might be produced by fluctuations in the surface potential, or they could have the form of traps lying deep in the oxide. We found in Sec. 3 that the localized states in gapless  $\text{Hg}_{1-x}\text{Cd}_x\text{Te}$  MOSFETs also influence the  $C$ - $V$  characteristics for  $f$  up to 5 MHz. This would indicate that the lifetime at  $T = 4.2$  K is unusually short, even for dielectric states.

Except for the heavily doped samples 5 and 9 (for which  $|N_A - N_D| \sim 10^{18} \text{ cm}^{-3}$ ), electron-trapping states were present in all of the samples. The reverse inequality  $N_s < n_s$  was satisfied for the heavily doped samples, which indicates that in this case states were present which supplied electrons to the inversion layer as the inversion-induced band bending increased. States in the depletion layer could provide the electrons in heavily doped  $p$ -type materials; indeed, because  $E_g$  is small (or even equal to zero for gapless materials), the strong electric field produced when  $V_G$  increases could facilitate electron tunneling from these states into the inversion layer without changing the total charge in the SCR.

Table I presents the subband filling rates  $dn_i/dn_s$  and the densities  $n_{si}$  at the start of the  $i$ th subband. Note that  $dn_i/dn_s$  for  $i = 1, 2$  is independent of the composition  $x$  and doping concentration. The subband populations were essentially the same for the lightly doped samples 1–3, which had similar compositions. This is fully consistent with the low surface charge density of acceptors in the depletion layer of sample 3 ( $N_d \approx 3 \cdot 10^{10} \text{ cm}^{-2}$ )—the charge did not materially alter the potential in the inversion layer even for  $n_s > 10^{11} \text{ cm}^{-2}$ .

It will be of interest to compare the data for samples 1 and 5. According to Table I, the depletion layer with

$N_d = 1.8 \cdot 10^{12} \text{ cm}^{-2}$  present in sample 5 increased the starting concentrations  $n_{s1}$  and  $n_{s2}$  more than tenfold without appreciably changing the filling rates  $dn_i/dn_s$ , provided the surface concentration  $n_s$  was such that samples 1 and 5 both had the same number of filled subbands.

## 5. CYCLOTRON MASSES AND THE ENERGY STRUCTURE OF THE SUBBANDS

For widegap semiconductors like Si and GaAs, the position of the bottom of the  $2D$ -subbands relative to the Fermi surface can be found directly from the surface density  $n_s$  of the carriers and the two-dimensional density of states  $D = m/\pi\hbar^2$ . (For Si and GaAs,  $D$  is independent of the energy and the effective mass  $m$  is the same as for a three-dimensional band).

By contrast,  $m$  depends on the electron density in the subbands and on the subband energies in narrow-gap semiconductors. There are two reasons why the cyclotron masses  $m_{ci}$  differ for the different subbands: a) the masses at the bottom of the subbands differ because the energy positions relative to the nominal bottom of the conduction and near the surface are not the same; 2) the Fermi energies differ.

As in the case of Shubnikov-de Haas oscillations, we can use our experimental technique to find the effective cyclotron masses by analyzing the oscillation amplitudes of the capacitance as  $T$  varies. Table I presents the measured results for  $n_s = 2 \cdot 10^{12} \text{ cm}^{-2}$ , and Fig. 4  $m_{ci}(n_s)$  plots for sample 6 (the one with the most filled subbands). We did not detect any significant structural changes in  $C(H)$ , nor in the position of the oscillation peaks near the phase jumps as  $T$  varied over the experimental range  $4.2 \leq T \leq 40$  K. This indicates that the subband populations were unchanged. The  $m_{ci}(n_s)$  dependence for the excited subbands in the other samples (with  $n_s > 2 \cdot 10^{12} \text{ cm}^{-2}$ ) was the same as for sample 6

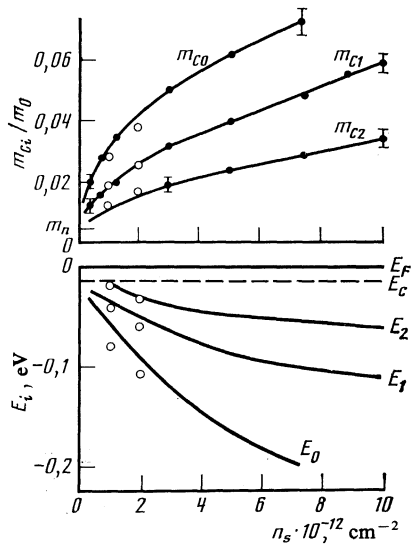


FIG. 4. Effective cyclotron masses and binding energies as functions of  $n_s$  for sample 6; the open circles  $\circ$  show values calculated in Ref. 3.

to within the experimental error—the maximum difference  $\approx 10\%$  in  $m_{c0}$  (for the lowest subband) occurred for sample 9, for which  $n_s = 8 \cdot 10^{12} \text{ cm}^{-2}$ .

According to Kane's model (where to lowest order we can neglect the  $\Gamma_7$ -band for our samples), the equations

$$n_i = \frac{m_{ni}}{\pi \hbar^2} (E_F - E_i) \left( 1 + \frac{E_F - E_i}{E_{gi}} \right);$$

$$m_{ci} = m_{ni} \left[ 1 + 4 \frac{E_F - E_i}{E_{gi}} \left( 1 + \frac{E_F - E_i}{E_{gi}} \right) \right]^{1/2} \quad (4)$$

express the densities  $n_i$  and cyclotron masses  $m_{ci}$  in terms of the Kane parameters  $E_{gi}$ ,  $m_{ni}$  and the energy difference  $E_F - E_i$  between the Fermi surface and the  $i$ th subband. Figure 4 shows the band parameters  $E_{gi}$ ,  $m_{ni}$ , and  $E_F - E_i$  (the energy position of the bottom of the  $i$ th subband) for sample 6; these results were found by assuming that  $E_{gi}$  and  $m_{ni}$  obey the same relation

$$E_{gi}/m_{ni} = E_g/m_n = 4P^2/3\hbar^2$$

as the corresponding bulk parameters  $E_g$  and  $m_n$  and by substituting the experimental values for  $n_i$  and  $m_{ci}$ . The relative energy  $E_F - E_i$  for the other lightly doped samples with  $n_s > 2 \cdot 10^{12} \text{ cm}^{-2}$  was similar to the results shown for sample 6;  $E_F - E_i$  differed by  $\lesssim 10\text{--}15\%$  for the heavily doped materials, which was comparable to the experimental error. Although  $E_F - E_i$  tended to increase somewhat in materials with narrower gaps  $|E_g|$ , the maximum increase was less than  $10\text{--}15 \text{ meV}$ . We see that for fixed  $n_s$  between  $3 \cdot 10^{12} \text{ cm}^{-2}$  and  $5 \cdot 10^{12} \text{ cm}^{-2}$ ,  $m_{ni}$ ,  $E_{gi}$ , and the energy separations  $\Delta E_{ij} = E_i - E_j$  are almost independent of the composition and doping of the samples.

A self-consistent theory was developed in Refs. 1 and 2 for calculating the populations of the electron states in inversion layers in narrow-gap semiconductors; calculated results for  $\text{Hg}_{1-x}\text{Cd}_x\text{Te}$  ( $x > 0.16$ ) were presented in Ref. 3. The curves  $n_i(n_s)$  given there for  $\text{Hg}_{0.78}\text{Cd}_{0.22}\text{Te}$  can be compared with our data for sample 3, whose composition was

similar. The theory predicts that four  $2D$ -subbands will be filled if  $n_s > 6 \cdot 10^{11} \text{ cm}^{-2}$ , whereas the experimental results imply that only three subbands are filled even for  $n_s \approx 10^{13} \text{ cm}^{-2}$ . The calculated  $n_{si}$  are also considerably less than the observed initial densities, and the population rate and the cyclotron masses for the  $i = 0$  subband are somewhat too low.

The usual ambiguity in determining the boundary conditions for the wave functions near the oxide interface could be responsible for the discrepancy between the experimental and theoretical results. Alternatively, the two-band approximation employed in Ref. 3 may be inadequate. In either case, we can expect the discrepancies to be greatest for the  $i = 0$  subband, because it is the most sensitive to the choice of the boundary conditions and because  $E_F - E_{i=0}$  is large, so that the two-band approximation tends to break down. Indeed, Table I shows that the experimental and calculated values for the excited subband ( $i > 0$ ) agree to within the experimental error. Moreover,  $m_{ci}$  and  $dn_i/dn_s$  for  $i > 0$  are independent of the composition, again in agreement with the theory,<sup>3</sup> which predicts a weak dependence on  $E_g$  for  $E_g < 0.1 \text{ eV}$ .

The resonant nature of the states near the surface must be taken into account for materials with  $E_g < 0.08 \text{ eV}$  (and all the more for gapless semiconductors), and here the theory runs into serious difficulties.<sup>3</sup> The contribution from surface and bulk state mixing to the energy spectrum of dimensionally quantized surface layers can be assessed qualitatively by comparing the results for samples whose Kane parameters  $E_g$  are equal in magnitude but opposite in sign. For small  $|E_g| < (0.1\text{--}0.2) \text{ eV}$  the dispersion laws will be similar in both samples; however, the wave functions corresponding to states in the surface conduction and bulk valence bands will overlap much more extensively in the sample with  $E_g < 0$ . If mixing is important, we thus expect to see a difference in the parameters of the  $2D$ -subbands for the two samples.

The absolute gapwidths  $|E_g|$  in our experiments were most nearly equal for samples 1 and 8. Although the bulk electron densities differed in the two samples, this is unimportant because the quantum effects of interest are caused by the degeneracy of the bulk electrons and affect only the starting concentrations  $n_{si}$ , whereas  $dn_i/dn_s$  and  $m_{ci}$  in the accumulation layers are quite insensitive to the doping level. According to Table I,  $dn_i/dn_s$  and  $m_{ci}$  (for all three subbands  $i = 0, 1, 2$ ) were the same for both samples to within the measurement error. The mixing of the majority and minority carrier bands thus had little influence on the energy spectrum of the  $2D$ -subbands.

The experimentally measured energies  $E_i$  are somewhat higher than the values predicted by the theory; however, the energy spacings  $\Delta E_{ij}$  between the subbands are close to the theoretical values (the discrepancy is less than the experimental error). Moreover,  $\Delta E_{ij}$  was found to be almost independent of the composition for fixed  $n_s = \text{const}$ , in full agreement with the theory.

The self-consistent theory developed in Refs. 1 and 2 thus provides a satisfactory description of the energy spectrum of quasi-two-dimensional surface electrons in narrow-gap and gapless  $\text{Hg}_{1-x}\text{Cd}_x\text{Te}$ . The theoretical results for

the excited subbands are in good quantitative agreement with experiment; however, the theory needs to be refined for the  $i = 0$  subband.

## 6. CONSEQUENCES OF DEGENERACY OF THE BULK ELECTRONS

Because the binding energy  $E_i - E_c$  for the  $i$ th  $2D$ -subband is  $\leq 0$  (where  $E_c$  is the energy of the bottom of the conduction band in the bulk of the semiconductor), the Fermi energy  $E_F - E_i$  in the two-dimensional subbands of degenerate materials cannot be less than the Fermi energy  $E_F - E_c$  for the bulk carriers.<sup>11</sup> Consequently, the surface density of the carriers at the start of the  $i$ th  $2D$ -subband must jump from  $n_i = 0$  to some threshold value  $n_i = n_t$ . We can find the threshold density by noting that the band parameters  $E_{gi}$  and  $m_{ni}$  coincide with their bulk values near the start of the subbands, so that the dispersion laws for the  $2D$ -subbands and the bulk material are also the same. Since the Fermi energies are also equal, we must also have  $k_{Fi} = k_F$ , where  $k_{Fi}$  and  $k_F$  are the quasimomenta corresponding to the Fermi energy in the  $2D$ -subbands and in the bulk. If we recall that  $k_{Fi}^2 = 2\pi n_i$ , and  $k_F^3 = 3\pi^2 n$  for a degenerate electron gas, we get the expression

$$n_i = (9\pi/8)^{1/3} n^{2/3}. \quad (5)$$

for  $n_i$  in terms of the bulk electron concentration  $n$ . The existence of a surface electron density threshold in the  $2D$ -subbands is apparent from the  $n_i(V)$  curves in Fig. 5. The lowest observable surface densities  $n_i = (2.1 \pm 0.1) \cdot 10^{11} \text{ cm}^{-2}$  coincide with the threshold  $n_t = 2.07 \cdot 10^{11} \text{ cm}^{-2}$  calculated by (5). Formula (5) is accurate for all of the degenerate  $n$ -type samples that we studied (samples 2, 6–8) and can be used to calculate  $n$  locally.

Figure 5 shows that the  $n_i(V)$  curves for the lower subbands are continuous for  $V$  corresponding to the start of excitation of the next higher subband. The surface potential therefore varies continuously with  $V$ , and hence so does the total induced charge  $N_s$ . On the other hand, the electron density  $n_s = \sum_i n_i$  in the  $2D$ -subbands jumps discontinuously by  $n_t$  at  $V = V_{si}$ .

This apparent contradiction is resolved by the theory<sup>7,8</sup> of surface screening in doped semiconductors. This problem was considered in Ref. 9 for InAs. According to Ref. 8, the self-consistent potential must vary continuously with the gate voltage  $V$  even if two-dimensional subbands are formed (we have already seen that in this case the concentrations jump discontinuously if the semiconductor is degenerate). The cause of this discontinuity is that the increase in the electron density in the surface subbands is exactly cancelled by a corresponding decrease in the surface density of free electrons.

We can use the experimental values  $n_s(V)$  and  $N_s(V)$  to calculate the surface density  $n_m$  of the free electrons:  $n_m = N_s - n_s$ . However, it is difficult to find the gate voltage corresponding to  $N_s = 0$ . For lightly doped samples, the  $n_i(V)$  curves all begin at the same cutoff voltage, which is equal (to within the experimental error) to the flat-band voltage deduced from the  $C-V$  measurements. On the other hand,  $V_{si}$  ( $i = 0, 1, 2$ ) are all different for the degenerate sam-

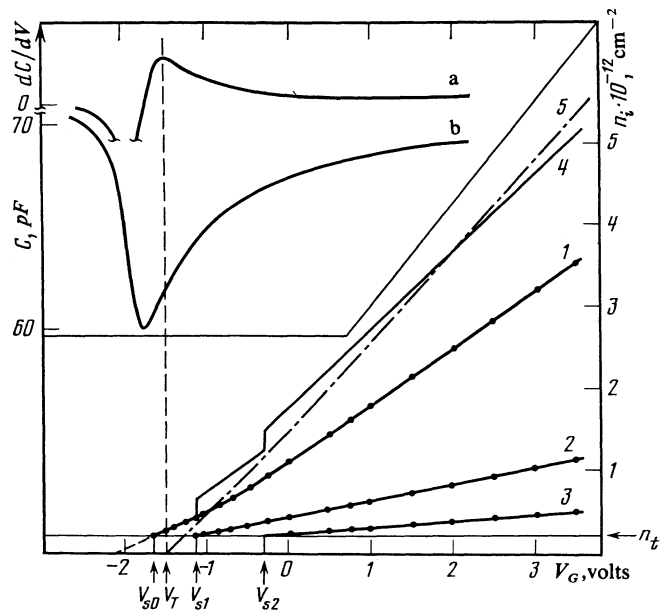


FIG. 5. Dependence of  $n_i$  (curves 1–3),  $n_s$  (4),  $N_s$  (5)  $dC/dV_G$  (a), and  $C$  (b) on the gate voltage  $V_G$  for sample 8.

ples (see Fig. 5), and in addition the band bending caused by the inversion is considerable for these voltages (see the  $C-V$  characteristics  $a$  and  $b$  in Fig. 5). The fact that the experimental and calculated values of  $n_i$  agree implies that the flat-band condition  $\varphi_s = 0$  corresponds to the starting voltage  $V_{s0}$  for the lowest subband. Although the classical approximation (valid for light doping) implies that the conditions  $\varphi_s = 0$  and  $N_s = 0$  are equivalent, the theory in Refs. 7 and 8 shows that for heavily doped materials,  $N_s = 0$  does not imply  $\varphi_s = 0$ . The value of  $\varphi_s = 0$  corresponding to  $N_s = 0$  can be found from Eq. (7.9) in Ref. 8; it was equal to 15.7 meV for sample 8. We can use this result and the calculated  $V(\varphi_s)$  dependences to find  $V - V_{s0}$  when  $N_s = 0$ . The result  $V - V_{s0} \approx 130 \text{ mV}$  for sample 8 is equal (to within the experimental error) to the “flat-band” voltage  $V_{FB}$  deduced from the  $C-V$  characteristics. A similar agreement holds for the other degenerate materials.

However, further studies are required here because the result for  $V_{FB}$  is based on a classical analysis of the  $C-V$  curves, according to which  $\varphi_s = 0$  when  $N_s = 0$ . When quantum effects are significant an SCR-capacitance of theory that includes dimensional quantization and electron-degeneracy effects will be needed in order to rigorously determine the values of  $N_s$  and  $\varphi_s$  corresponding to the classically determined  $V_{FB}$ . The successful theory of the future will also have to treat the effects caused by the nonparabolicity of the  $\Gamma_6$ - and  $\Gamma_8$ -bands for narrow-gap and gapless semiconductors; these semiconductors are of particular interest, because their high Fermi energies and large Bohr radii create conditions especially favorable for observing electron degeneracy effects.

## 7. OSCILLATIONS IN THE SCREENING LENGTH WITH VARYING MAGNETIC FIELD

Measurements in oblique magnetic fields show that the field component normal to the oxide interface determines

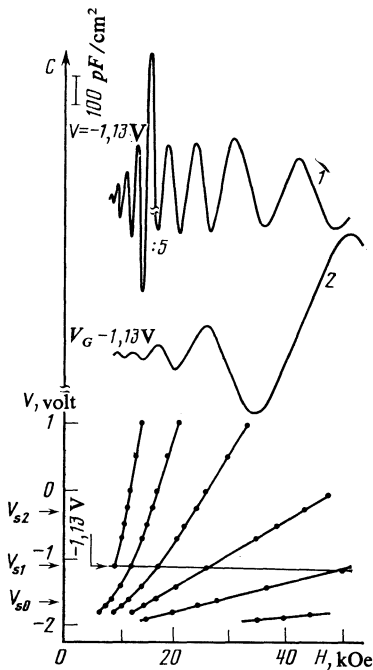


FIG. 6. Magnetooscillations of the capacitance for magnetic fields normal (1) and parallel (2) to the surface for sample 8. The peak positions are also plotted as a function of voltage for a parallel field ( $\alpha = \pi/2$ ).

the capacitance-oscillation periods. We recall that these oscillations are a consequence of the quantization of the energy spectrum of the two-dimensional electrons by the magnetic field. In the extreme case of zero normal component ( $\alpha = \pi/2$ ), there is no Landau quantization in the  $2D$ -subbands and no oscillations should be observed. Indeed, in general none were found. However, the heavily doped  $n$ -type samples 2, 6–8 constitute an exception; their capacitance oscillated even at parallel  $H$  for gate voltages from somewhat less than the start voltage for the lowest subband to voltages corresponding to surface densities  $\sim (3-5) \cdot 10^{12} \text{ cm}^{-2}$ . Figure 6 shows the  $C(H)$  oscillation maxima for this orientation of  $H$  and for various  $V$ . It shows also the  $C(H)$  curves for parallel and perpendicular magnetic fields. The oscillations were periodic in  $1/H$  for all  $V$  at  $H$  parallel, and when the oscillation phases varied with  $V$ , the periods were nearly independent of  $V$  and coincided to within the experimental error with the SdH oscillation period measured for the initial  $\text{Hg}_{1-x}\text{Cd}_x\text{Te}$  wafers. This suggests that Landau quantization of three-dimensional electrons is responsible for the oscillations.

One can show easily that for degenerate materials, oscillations of the screening length  $L$  should cause  $C(H)$  to oscillate near the flat-band voltage regardless of the field orientation. If  $e\varphi_s \ll E_F - E_c$  (linear screening approximation),  $L$  is determined by the density of states at the Fermi level.

$$L = (e/4\pi e^2)^{1/2} (dn/dE_F)^{-1/2}.$$

Since  $dn/dE_F$  oscillates for a degenerate electron gas in a quantizing magnetic field, so will  $L$ .

On the other hand, we also have  $e\varphi_s \ll E_F - E_c$  near the flat-band voltage, if the system is highly degenerate, and if

we neglect the minority carrier charge and the quantum effects considered in Sec. 6 we have the expression

$$Q_s = e \int_{\varphi_s}^0 \frac{dn}{dE_F} \left( \frac{d\varphi}{dz} \right)^{-1} \varphi dz$$

for the charge density in the SCR. Here  $\varphi(z)$  is the band bending at a point at a distance  $z$  from the surface. Using the linearized Poisson equation to evaluate  $d\varphi/dz$ , we find

$$C_s = \frac{dQ_s}{d\varphi_s} = e \left( \frac{\epsilon}{4\pi} \right)^{1/2} \left( \frac{dn}{dE_F} \right)^{1/2} = \frac{\epsilon}{4\pi L}$$

for the capacitance of the SCR. This result implies that if  $e\varphi_s < \hbar\omega_c$ , the magnetic quantization of the bulk-electron spectrum will cause the SCR capacitance to oscillate; moreover, unlike the oscillations due to quantization of a two-dimensional gas of surface electrons, the screening oscillations will occur for arbitrary orientations of the magnetic field.

However, the above semiclassical analysis cannot explain why  $C(H)$  oscillates for voltages  $V \gg V_{FB}$  when  $\alpha = \pi/2$ . At these voltages the band curvature is so great that the external field is screened primarily by the charge of the electrons in the  $2D$ -subbands; since these electrons are constrained to move two-dimensionally, they should not give an oscillatory contribution to the screening when  $\alpha = \pi/2$ . However, oscillations are observed for gate voltages  $V_G$  corresponding to strong accumulation. This indicates that some of the screening must be due to continuum states which are either free or only weakly bound in the  $z$  direction (these were considered in Sec. 6).

We have pointed out that as  $V$  increases above  $V_{FB}$ , the phases of the oscillations in  $C(H)$  change but the period stays the same; moreover, the phase changes by almost  $2\pi$  as  $V$  increases from  $V_{si}$  to  $V_{si+1}$ . We regard this as an experimental manifestation of Levinson's theorem,<sup>10</sup> which predicts that the phase of the wave function of continuum states will change by  $\pi$  when the next bound state forms in the discrete spectrum. We do not know of any other experimentally observable consequences of this result.

Similar behavior was previously observed for weakly degenerate InAs ( $\alpha = \pi/2$ ) in Ref. 11, where it was attributed to successive emptying of the hybrid surface subbands, which were pushed up above the Fermi level by the diamagnetic energy shift caused by the parallel magnetic field. However, this mechanism cannot explain the observed oscillations in  $C(H)$ , because it is inconsistent with our findings for the heavily doped samples. Specifically: 1)  $C(H)$  oscillated for  $V < V_{s0}$ , i.e., when there were no two-dimensional subbands even at  $H = 0$ ; 2) for all  $V$  the number of oscillations exceeded the number of filled subbands; 3) no oscillations in parallel fields  $H$  were observed in weakly doped accumulation layers, nor in inversion layers; 4) when the inclination angle  $\alpha$  varied, the oscillation periods changed at the same rate for all of the  $2D$ -subbands, which indicates that the component of  $H$  parallel to the surface had no influence on the carrier density ratios for the different subbands; 5) the oscillation periods were nearly equal to the SdH oscillation periods, i.e., three-dimensional bulk carriers were involved. A separate investigation beyond the scope of this paper will be

required for a more detailed analysis of the experimental results on accumulation layers in oblique magnetic fields.

## 8. SPIN SPLITTING

Because of the strong spin-orbit interaction and the small gapwidth  $E_g$ , the effective  $g$ -factor of the bulk electrons in our samples was as high as 100–250, and the spin splitting comprised nearly 50% of the orbital splitting, as opposed to  $\sim 20\%$  in silicon. This difference should be even greater when a two-dimensional electron gas is present. Indeed, multielectron effects are important in Si, and the  $g$ -factor is fairly insensitive to the energy; moreover, the exchange energies differ for carriers with like and unlike spin orientations, so that for small  $n_s$  the paramagnetic splitting in Si inversion layers is substantially greater than in bulk Si, and the splitting decreases as  $n_s$  increases.<sup>12</sup> By contrast, the nonparabolic band profiles are the determining factor for two-dimensional electron gases in narrow-gap semiconductors. For materials with a Kane dispersion law, we have the expression<sup>13</sup>

$$g_e = -\frac{m_0}{m_c} \frac{2\Delta}{[3(E_F - E_c) + 3E_g + 2\Delta]} \quad (6)$$

for the  $g$ -factor at the Fermi level in terms of the effective cyclotron mass  $m_c$ . (Note that it is the  $g$ -factor which is measured experimentally, whether one studies SdH oscillations or oscillations in the capacitance of the SCR.) We have  $\Delta = E(\Gamma_8) - E(\Gamma_7)$  in Eq. (6), and we must set  $E_g = 0$  for negative gaps  $E_g < 0$ . If we assume that (6) remains valid for two-dimensional subbands, the measured  $m_{ci}$  imply that in narrow-gap materials, the  $g$ -factor for the surface electrons must be less than in the bulk and must decrease as the surface concentration  $n_s$  increases; the ratio  $g_{\text{bulk}}/g_{\text{surf}}$  may reach several times ten for  $n_s \sim 10^{13} \text{ cm}^{-2}$ .

For our samples, spin splitting of the capacitance oscillations cannot occur except in the lowest subband of materials with  $E_g > 0$ . Figure 7 shows some oscillation curves for sample 3, together with a fan diagram of the Landau levels for small negative applied voltages  $V_G$  (weak accumulation). We note that spin splitting was observed for  $n_s < (1-1.5) \cdot 10^{12} \text{ cm}^{-2}$  in the range of magnetic fields investigated, but only for Landau levels with  $N \leq 3$ . An analysis of the positions of the oscillation maxima and minima along the  $1/H$  axis (see, e.g., Fig. 2) shows that  $s = -1/2$  for the unsplit oscillations ( $N > 3$ ), as can also be clearly seen from Fig. 7.

The behavior of the state density function directly determines the oscillations of the capacitance. Levels with the high-field  $s = +1/2$  spin are very susceptible to nonthermal broadening, which apparently explains why the Landau levels with  $N > 3$  all have  $s = -1/2$ . Further support for this explanation is provided by the finding that the oscillation amplitude for levels with  $s = +1/2$  is considerably more sensitive to  $H$  than for  $s = -1/2$ .

Oblique magnetic fields<sup>12</sup> are used to measure the  $g$ -factor in Si inversion layers. This technique exploits the fact that the orbital splitting in a two-dimensional gas is determined by the component  $H_{\perp} = H \cos \alpha$  normal to the interface, whereas the spin splitting depends on the magnitude  $H = (H_{\perp}^2 + H_{\parallel}^2)^{1/2}$  of the complete field. This method must

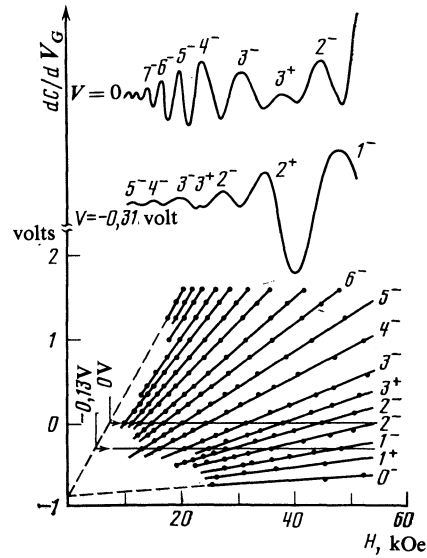


FIG. 7. Magnetooscillations in  $dC/dV_G$  (top) and peak positions as a function of  $V_G$  (bottom) for sample 3.

be modified for narrow-gap materials, because the strong spin-orbit coupling in general makes the spin splitting depend on the field orientation.

In order to clarify this question we studied the oscillations in  $C(V)$  by varying  $H$  with  $\alpha = \text{const} = 0$  (so  $H_{\perp} = H$ ), and by varying  $\alpha$  with  $H = \text{const}$  ( $H_{\perp} = H \cos \alpha$ ). The fan diagram of the Landau levels recorded in the first case was of course similar (up to phase) to the diagram shown in Fig. 6. In general, the excited subbands do not significantly distort the structure of the levels; in any case, we eliminated possible distortions by measuring the positions of the capacitance maxima in terms of  $n_0$  rather than  $V$ . Here  $n_0$ , the surface density in the lowest subband, was deduced from the oscillation periods of the  $(dC/dV)(H)$  dependence. Figure 8 shows the values of  $n_0$  corresponding to peaks in  $C(V)$ ; the maximum field,  $H = H_{\perp} = H_{\text{max}} = 54 \text{ kOe}$ , is indicated on the horizontal axis. In order to keep from cluttering the figure, the vertical axis plots  $n_0(H_{\text{max}}/H_{\perp})$  rather than the actual value  $n_0$  for fields  $H = H_{\perp} < 54 \text{ kOe}$ . This rescaling transforms the fan diagram described by (1) into a system of parallel levels for  $\alpha = \text{const}$ . We see from Fig. 8 that the rescaled levels are in fact parallel, except for  $H < 35 \text{ kOe}$ , where the spin splitting is poorly resolved.

We used the same procedure to construct the fan diagram by changing  $H_{\perp}$  by rotating a magnetic field with  $H = \text{const} = H_{\text{max}}$ . If the spin splitting depended only on  $H_{\perp}$ , the fan diagram should be the same as when  $\alpha = 0$ . However, the actual diagrams differed significantly—when  $\alpha$  was kept equal to 0 and  $H_{\perp}$  was changed by varying  $H$ , the relative positions of the levels in Fig. 8 did not change; however, when  $H_{\perp}$  was varied by changing  $\alpha$  ( $H = \text{const} = H_{\text{max}}$ ), the relative spacing between the spin-split Landau levels  $N^+$ ,  $N^-$  increased, while the spacing between the levels  $N^-$  and  $(N+1)^+$  became smaller. As  $\alpha$  increased, the position of the unsplit  $N^-$  levels ( $N > 3$ ) changed, indicating a change in the oscillation phase; however, the relative spac-

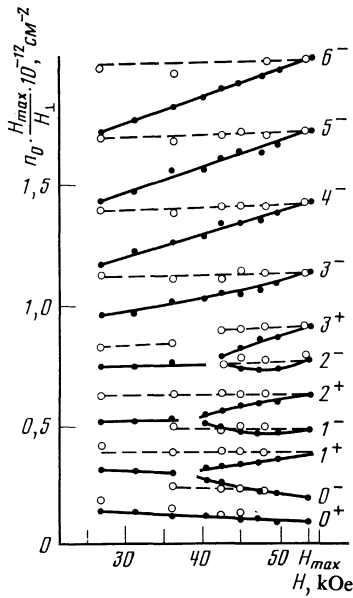


FIG. 8. Positions of the peaks in  $C(V)$  for sample 3. The results are expressed in terms of  $n_0 H_{\max} / H_1$  and  $H$  for fields making an angle  $\alpha$  with the normal to the surface ( $H_{\max} = 54$  kOe). Solid curves:  $H_1 = \cos \alpha$ ,  $H = \text{const} = H_{\max}$ ; dashed lines:  $H_1 = H$ ,  $\alpha = 0$ .

ings between the orbitally split levels  $N^-$ ,  $(N+1)^-$  and  $N^+$ ,  $(N+1)^+$  were independent of  $\alpha$  (the pair  $0^+$  and  $1^+$  is an exception). The magnitude of the field causing the spin splitting can be deduced from the relative spacings between the oscillations observed for the two opposite spins when  $H_1 = H \cos \alpha$  was varied. We found that just as for Si, the total magnetic field  $H = (H_{\parallel}^2 + H_{\perp}^2)^{1/2}$  determined the magnitude of the spin splitting in all samples where spin levels were observed.

We can therefore find the electron  $g$ -factor for the lowest subband by measuring the angle  $\alpha$  at which the oscillations in the split subbands are equidistant, i.e., the angle for which the spin splitting is equal to one-half the cyclotron splitting:  $|g| \mu_B H = (\hbar e H / 2m_{c0} c) \cos \alpha$ .

We found that  $\alpha = (25 \pm 3)^\circ$  regardless of the value of  $n_s$ . Our result  $|g_{c0}| = 0.9m_0/m_{c0}$  for the  $g$ -factor is in good agreement with Eq. (6), which gives a numerical factor of 0.87 for our materials. In other words Eq. (6) remains valid in the two-dimensional case, at least for  $n_s < 10^{12} \text{ cm}^{-2}$ .

No spin splitting was observed for negative-gap materials ( $E_g < 0$ ). We can think of two possible explanations: 1) the splitting was too small to be resolved (this seems unlikely, since the bulk  $g$ -factor for these samples is larger than for positive-gap materials,  $E_g > 0$ ); 2) one of the spin components might not have shown up, because the corresponding energy level was excessively broadened. The latter explanation is supported by the finding that the oscillation phases were similar to those observed for the series of  $s = -1/2$  levels in the positive-gap samples, and the dependence of the phases on  $\alpha$  was also similar.

The "extinction" of the high-field ( $s = +1/2$ ) spin component in narrow-gap and gapless materials at certain orientations  $\alpha$  was noted previously in Refs. 6, 14, and 15,

where oscillations caused by three-dimensional effects were studied. Our results imply that similar behavior can also occur in two-dimensional systems in magnetic fields. Since these results are based on capacitance measurements, they indicate that the state densities differ for levels with unequal magnetic moments (e.g., for levels with different degrees of collisional broadening). We see that as the density of ionized impurities increases, the width of the  $s = +1/2$  and  $s = -1/2$  levels behaves differently for samples 1 and 5. The Landau levels with  $N \leq 3$  show a distinct spin splitting in the first case; on the other hand, for sample 5 no high-field spin component was present in the oscillations for  $N = 1-3$  (recall that sample 5 was obtained from 1 by heating, which increased the acceptor concentration  $N_A$ ). On the other hand, the behavior of the low-field components was similar for both samples.

We see by comparing the results for samples with different Cd contents  $x$  that the difference between the amplitudes of the spin-split oscillations increases greatly upon transition from a direct to an inverted band structure, i.e., as the  $p$ -type  $\Gamma_8$ -band becomes more important in the energy spectrum of the conduction band. This behavior may be attributed to scattering of the  $\Gamma_8$ -band carriers in the magnetic field. However, additional theoretical work will be needed to understand why the spin-split Landau levels  $N^+$ ,  $N^-$  are not broadened to the same extent.

## 9. LOCALIZATION IN A MAGNETIC FIELD

The oscillations for each spin series were periodic in  $1/H$  for all  $H$  in the weakly doped positive-gap samples for which spin splitting was observed. On the other hand, no splitting was observed at higher doping levels  $|N_A - N_D| > 10^{15} \text{ cm}^{-3}$  in either positive- or negative-gap materials (sample 5, samples 6-8, respectively), and the periodicity broke down for large  $H$  (Fig. 9). For all  $n_s$ , the oscillations corresponding to Landau levels with  $N \leq 2$  occurred at lower fields than predicted by (1) for a constant surface carrier density  $n_0$  in the lowest subband. The studies in oblique magnetic fields indicate that the component  $H_{\parallel}$  parallel to

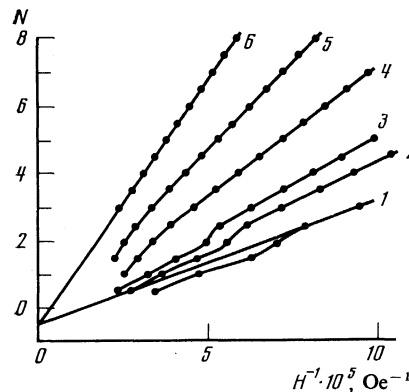


FIG. 9. Fan diagram for the oscillations  $C(H)$ , plotted along the  $H^{-1}$  axis;  $N$  is the number of the Landau level corresponding to a given extremum (half-integral  $N$  correspond to minima). For sample 6 and gate voltages  $V_G = -1.3$  (1),  $-1.2$  (2),  $-1.15$  (3),  $-1.0$  (4),  $-0.8$  (5) and  $-0.5$  V (6).

the surface has no effect on the structure of the oscillations. On the other hand, the departures from periodicity were the same for both the lightly and the heavily doped samples and were observed for  $n_s$  both larger and smaller than the threshold for subband excitation; this suggests that as in silicon,<sup>16,17</sup> localization of carriers in the magnetic field decreases  $n_0$  and thereby destroys the periodicity.

The surface density  $n^{im}$  of carriers in these localized states is equal to the difference  $n_0 - n_0^m$  when the magnetic field  $H_N$  corresponds to a minimum in the capacitance, i.e., is such that the Fermi level passes midway between the  $N$  and  $N - 1$  Landau levels;  $n_0$  is the carrier density in the lowest subband (determined from the periods  $\Delta_i$  for  $N > 2$ , for which the localization effects are unimportant);  $n_0^m = g_s(eH_N/ch)N$  is the density of mobile carriers in  $N$  completely filled Landau levels. We can find  $n_0^m$  as a function of the magnetic field  $H$  by determining  $n_0$  for various gate voltages (i.e., by considering the different fields  $H$  for which  $C(H)$  has a minimum). The experimental dependences  $n_0^m(H)$  for  $N = 1, 2$  were different for samples 5, 7, and 8; they are described approximately by the relation<sup>17</sup>

$$n_0^m = (g_s e H / ch) (2N + 1)^{-1},$$

which holds for Si inversion layers. The Landau-level filling factors  $\nu = n_0 ch / g_s e H$  corresponding to the peaks in the  $C$  are given approximately by

$$\nu = 1 \frac{1}{3} (N=1), \quad \nu = 2 \frac{1}{5} (N=2),$$

which follows from the above formula for  $n_0^m$ . For sample 6 we have

$$n_0^{im} = 1/3 g_s e H / ch$$

for both  $N = 1$  and  $N = 2$ , which corresponds to filling factors  $\nu = 4/3$  and  $7/3$ , respectively. We note that the  $N = 1, 2$  Landau levels were also observed in the  $i = 1$  subband in sample 5; however, the oscillations for  $N < 3$  remained periodic for all  $H$ . We thus conclude that Anderson localization induced by the magnetic field was responsible.<sup>16</sup> Indeed, the experimental results show that localization was important only for heavily doped samples (with the highest density of states at the oxide interface or in the depletion layer), which suggests that fluctuations in the potential were responsible.

In some cases we observed an additional oscillatory structure ( $i = 0, N = 1, 2$ ) for sample 6, which was the most lightly doped of the samples 5–8 considered here (its bulk electron mobility was  $\sim 10^6$  cm<sup>2</sup>/V·s). Figure 10 shows these oscillations, which for  $H_{\perp} = \text{const}$  were independent of the field orientation  $\alpha$ ; the fields for which  $\nu$  is a multiple of  $1/3$  are also shown. The experimental minima in  $C(H)$  for  $N = 1, 2$  correspond closely to the values  $\nu = 4/3, 5/3, 6/3, 7/3, 8/3$  and may have the same physical origin as the fractional plateaus observed in the anomalous quantum Hall effect.

## 10. CONCLUSIONS

We may summarize our findings as follows.

1) We measured the magnetooscillations of the SCR capacitance in MOS structures and used the results to analyze the two-dimensional gas of surface electrons in  $n$ - and  $p$ -type

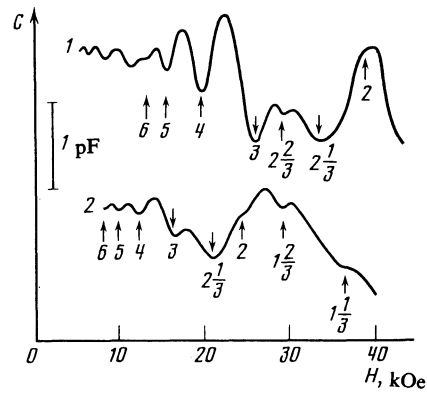


FIG. 10. Magnetooscillations in the SCR capacitance for sample 6,  $n_0 = 3.74 \cdot 10^{-11}$  cm<sup>-2</sup> (1),  $2.36 \cdot 10^{-11}$  cm<sup>-2</sup> (2). The arrows indicate the fields for which the filling factors  $\nu$  are multiples of  $1/3$ .

Hg<sub>1-x</sub>Cd<sub>x</sub>Te for surface densities  $n_s \leq 10^{13}$  cm<sup>-2</sup>. Specifically, we determined the densities, cyclotron masses, binding energies, and dispersion law (Kane parameters).

2) The properties of the two-dimensional electron gas are essentially the same in materials with direct or inverted band structures, provided the dispersion laws are similar. For the range  $0.09 \leq x \leq 0.22$  of Cd contents investigated, the bulk characteristics had little influence on the behavior of the 2D-subbands for surface carrier densities  $n_s > (3-5) \cdot 10^{12}$  cm<sup>-2</sup>.

3) Because of the large Fermi energy and Bohr radius, quantum effects are important in Hg<sub>1-x</sub>Cd<sub>x</sub>Te accumulation layers for both positive and negative  $E_g$ . Screening by unbound electrons appreciably alters the behavior of the oscillations for fields parallel to the surface.

4) The total magnitude  $H = (H_{\parallel}^2 + H_{\perp}^2)^{1/2}$  of the magnetic field determines the magnitude of the spin splitting in oblique fields for positive  $E_g$ , just as in the case of silicon. In contrast to wide-gap materials, however, the  $g$ -factor for the two-dimensional electron gas in Hg<sub>1-x</sub>Cd<sub>x</sub>Te ( $E_g > 0$ ) is less than for the bulk electrons and drops considerably as  $n_s$  increases. No high-field ( $s = +1/2$ ) spin component of the oscillations is observed for materials with  $E_g < 0$ .

5) Localization of the two-dimensional carriers by the magnetic field is important for heavily doped materials with  $|N_A - N_D| > 10^{15}$  cm<sup>-3</sup> and sets in at appreciably lower  $n_0$  and  $H$  than is the case for Si ( $n_0$  is the carrier concentration in the lowest subband). For the purest specimens with the highest electron mobility, the minima in  $C(H)$  occurred for Landau filling factors  $\nu$  equal to multiples of  $1/3$ .

We close by briefly discussing how the quantum Hall effect might be observed in narrow-gap semiconductors. Because these materials have large  $g$ -factors and small cyclotron masses, the splitting of the Landau levels is pronounced and occurs at weaker fields and higher temperatures than for Si or GaAs. However, our results indicate other characteristics of narrow-gap materials may make it difficult to observe the quantum Hall effect. Specifically, the localization (quantization) by the magnetic field is impaired because several subbands are present. The fact that the cyclotron masses increase with the surface concentration  $n_s$  is another nega-

tive factor. The high degree of nonthermal broadening of the high-field spin components of the Landau levels presents even more serious difficulties, because the "tails" of the broadened states may overlap with the neighboring energy levels so that the carriers are not confined to well-defined bands. The quantization of the Hall conductivity is seriously degraded even if the band tails contain only a low density of mobile states. According to our results, this degradation will be most severe for heavily doped materials with small  $|E_g|$ . On the other hand, there is a trade-off here because the starting concentration  $n_{si}$  for the subbands decreases if the doping concentration is decreased, while an increase in  $E_g$  will decrease the magnitude of the cyclotron and spin splittings. Additional work is needed to find optimum materials for observing the quantum Hall effect.

It is a pleasant duty to thank G. M. Min'kov, V. V. Kruzhaev, and O. É. Rut for calculating the band parameters for bulk  $Hg_{1-x}Cd_xTe$ , and Prof. I. M. Tsidil'kovskii for his interest in this work and for helpful discussions.

<sup>1)</sup>Here we neglect the diamagnetic shift in magnetic fields having a non-zero component parallel to the surface.

<sup>1)</sup>Y. Takada, K. Arai, N. Uchimura, and Y. Uemura, *J. Phys. Soc. Jpn.* **49**, 1851 (1980).

- <sup>2)</sup>G. E. Marques and J. L. Sham, "Electronic properties of two-dimensional systems," in: *Proc. Fourth Int. Conf. Surf. Sci.*, Vol. 113 (1982), p. 131.
- <sup>3)</sup>Y. Takada, K. Arai, and Y. Uemura, in: *Proc. Fourth Int. Conf. Phys. Narrow Gap Semicond.*, Lect. Notes Phys., Vol. 152, Springer-Verlag, New York (1982), p. 101.
- <sup>4)</sup>G. A. Antcliffe, R. T. Bate, and R. A. Reynolds, in: *Proc. Conf. Semimetals and Narrow Gap Semicond.*, Dallas (1971), p. 499.
- <sup>5)</sup>J. P. Vitton, J. P. Dufour, R. Machet, and Y. C. Thuillier, *Phys. Status Solidi (b)* **120**, K53 (1983).
- <sup>6)</sup>L. P. Zverev, V. V. Kruzhaev, G. M. Min'kov, and O. É. Rut, *Zh. Eksp. Teor. Fiz.* **80**, 1163 (1981) [*Sov. Phys. JETP* **53**, 595 (1981)].
- <sup>7)</sup>O. V. Konstantinov and A. Ya. Shik, *Zh. Eksp. Teor. Fiz.* **58**, 1662 (1970) [*Sov. Phys. JETP* **31**, 891 (1970)].
- <sup>8)</sup>G. A. Baraff and J. A. Appelbaum, *Phys. Rev.* **5**, 475 (1972).
- <sup>9)</sup>H. Reisinger, H. Schaber, and R. E. Doezema, *Phys. Rev.* **24**, 5960 (1981).
- <sup>10)</sup>L. D. Landau and E. M. Lifshitz, *Kvantovaya Mekhanika (Quantum Mechanics: Nonrelativistic Theory)*, 3rd. ed., Pergamon Press, Oxford (1977).
- <sup>11)</sup>R. E. Doezema, M. Nealon, and S. Whitmore, *Phys. Rev. Lett.* **45**, 1593 (1980).
- <sup>12)</sup>F. F. Fang and P. J. Stiles, *Phys. Rev.* **174**, 823 (1968).
- <sup>13)</sup>I. M. Tsidil'kovskii, *Zonnaya Struktura Poluprovodnikov (Band Structure of Semiconductors)*, Nauka, Moscow (1978), p. 238.
- <sup>14)</sup>S. Narita and K. Suizu, *Phys. Lett.* **43A**, 353 (1973).
- <sup>15)</sup>N. G. Gluzman, A. I. Ponomarev, G. A. Potapov, L. D. Sabirzyanova, and I. M. Tsidil'kovskii, *Fiz. Tekh. Poluprovodn.* **12**, 468 (1978) [*Sov. Phys. Semicond.* **12**, 271 (1978)].
- <sup>16)</sup>T. Ando, *J. Phys. Soc. Jpn.* **52**, 1740 (1983).
- <sup>17)</sup>T. Ando, A. B. Fowler, and F. Stern, *Rev. Mod. Phys.* **54**, 437 (1982).

Translated by A. Mason